The International Journal of Advanced Manufacturing Technology (2023) 125:967–987
https://doi.org/10.1007/s00170-022-10765-4

APPLICATION

# Machinability and chip morphology evolution of hardened stainless steel using liquid nitrogen cryogenic

**Wenyuan Wang[1] · Biling Wang[2] · Boyu Liu[2] · Hang Gao[1] · Zhaocheng Wei[1]**

Received: 20 September 2022 / Accepted: 22 December 2022 / Published online: 30 December 2022


## Abstract

The impeller material FV520B-hardened stainless steel is a typical difficult-to-machine material. During the cutting process, the force and thermal load are large, and the chip breaking is difficult, resulting in poor processing quality and serious tool wear. Low temperature cooling can improve the machinability of materials by significantly reducing the temperature of the cutting zone. It is an important development direction of clean cutting in the future. In this paper, the effects of low temperature cooling (18 ~ − 196℃) on cutting machinability and chip morphology evolution of FV520B were systematically studied from macroscopic and microscopic aspects by setting triaxial milling and orthogonal turning experiments respectively based on low-temperature jet formed by mixing liquid nitrogen and compressed air. The experimental results show that liquid nitrogen cryogenic cutting can significantly improve the machinability of material FV520B and promote the formation of serrated chips. Under the condition of cutting speed of 80 m/min, axial cutting depth of 1 mm and feed per tooth of 0.25 mm/r, the cutting force, cutting vibration, and surface roughness of FV520B at − 100℃ are reduced by 30%, 62%, and 18% respectively compared with those at 18℃. When the cutting speed is 80 m/min, the axial cutting depth is 1 mm, and the feed per tooth is 0.1 mm/z, the tool life at − 100℃ is 43% higher than that at 18℃. With the increase of cutting speed and the decrease of jet temperature, the serration degree, pitch, and shear angle of chips increase and the deformation coefficient of chips decreases.

**Keywords** The impeller · Hardened stainless steel · Low temperature cutting · Machinability · Chip morphology

## Nomenclature

| | |
|---|---|
| $QN$ | Flow of liquid nitrogen |
| $v$ | Cutting speed |
| $fz$ | Feed per tooth |
| $Ra$ | Surface roughness |
| $\xi$ | Chip deformation coefficient |
| $h$ | Tooth valley high |
| $G_s$ | Degree of chip serration |
| $\phi$ | Angle of shear |
| $\alpha$ | Inclination angle of adiabatic shear band |
| $E$ | Young's modulus |
| $\sigma_s$ | Yield strength |
| $HV$ | Hardness |
| $QA$ | Air flow |
| $a_p$ | Axial cutting depth |
| $T$ | Temperature of low temperature jet |
| $VB$ | Rear face wear amount |
| $H$ | Tooth peak height |
| $H-h$ | Depth of tooth |
| $L_p$ | Distance between adjacent chips teeth |
| $\delta$ | Width of adiabatic shear band |
| $\rho$ | Density |
| $v$ | Poisson's ratio |
| $R_m$ | Tensile strength |
| $\Psi$ | Section shrinkage |

✉ Zhaocheng Wei
wei_zhaocheng@dlut.edu.cn

[1] Key Laboratory for Precision and Non-Traditional Machining Technology of Ministry of Education, Dalian University of Technology, Dalian 116024, People's Republic of China

[2] AVIC Aerodynaiviics Research Institute, Shenyang 110086, People's Republic of China

## 1 Introduction

The cutting fluid used in the existing cooling process comes from non-renewable resources such as oil, and the cost of later purification treatment is high. Direct discharge will cause great pollution to the environment. At present, with

the development of refrigeration technology, clean cutting represented by low-temperature cutting has gradually become a research hotspot. Low-temperature cutting has no pollution to the environment and can change the mechanical properties of materials, promote the forced heat exchange in the cutting area, and improve the machinability of materials [1, 2].

Centrifugal compressor is widely used in petroleum, chemical industry, natural gas, metallurgy, and other fields. It is the core equipment of major engineering supporting devices [3]. As the "heart" of centrifugal compressor, the processing quality of impeller directly affects the efficiency of centrifugal compressor, and the processing efficiency and processing cost are related to great economic benefits. At present, the main machining method of impeller is NC cutting. In addition to the difficulties caused by complex geometric structure, the difficulty of material machining is an important factor restricting the high-quality and efficient machining of impeller [4, 5]. The cutting process of impeller material FV520B hardened stainless steel mainly has the following characteristics: (1) after heat treatment, the hardness reaches 40HRC, the cutting surface hardness is increased by 1.4 ~ 2.2 times, the work hardening is serious, and the cutting force is large; (2) The thermal conductivity is low, the cutting temperature is more than 200℃ higher than that of 45 steel, and the tool wear is serious; (3) The material has high plasticity and is easy to bond with the tool to form chip accumulation tumor, which reduces the quality of the cutting surface; (4) The material has high strength, and the chips are not easy to break and damage the cutting surface.

In this paper, the effects of different temperature conditions (18 ~ − 196℃) and cutting parameters at corresponding temperatures on the machinability and chip morphology evolution of FV520B hardened stainless steel were investigated. Scholars have carried out a series of studies on the factors affecting the machinability [6–9] and chip morphology evolution [10–13] of metal materials. These include processing parameters and cooling conditions. Akgün et al. [6] carried out hard turning experiments on AISI H13 tool steel using ceramic tools to explore the influence of cutting parameters on the machinability of materials. The results show that the feed rate has an important influence on the main cutting force and surface roughness, and the cutting speed has an important influence on the cutting power and cutting temperature. Altan Özbek et al. [7] turned Vanadis 10 by MQL and dry cooling. The results show that compared with dry machining, MQL has a significant improvement in cutting temperature, tool vibration amplitude, tool wear, and surface roughness. Pimenov et al. [8] extensively analyzed the literature on dry, conventional system, minimum quantity of lubricant cooling (MQL), cryogenic lubrication, and high-pressure cooling (HPC). Show the effects of various cooling methods on surface roughness, tool wear, tool life, temperature, and cutting force. The main advantages and disadvantages of different cooling methods are analyzed. Hegab et al. [10] investigated the effect of nano cutting fluid containing multi-walled carbon nanotubes (MWCNT) and aluminum oxide ($Al_2O_3$) on the machinability and chip morphology of Inconel718. The results show that MWCNT nanofluids exhibit better performance. Shi et al. [11] analyzed the influence of sampling direction and cutting speed on chip morphology of TC4 with obvious anisotropy. It was found that material direction and cutting speed had significant effects on chip morphology. The critical cutting speed of chip changing from serrated chips to fragmented chips was different when the direction ranged from 0° to 90°.

With the development of high-performance cutting equipment, the pursuit of processing efficiency, processing quality, processing cost, and environmental friendliness is increasing. The demand for more environmentally friendly and effective processing methods is increasing. In recent years, for different difficult machining materials, scholars have proposed some clean low-temperature cutting technologies with compressor refrigeration, liquid nitrogen, and supercritical carbon dioxide as cooling media. Sun et al. [14] compared low-temperature cooling cutting with dry cutting TC4 titanium alloy and found that the low-temperature cutting force was significantly reduced and the surface quality was improved. Liu et al. [15] investigated the effect of air-cooling on the machinability of TC4 titanium alloy. Results show that the air-cooling significantly provides lower cutting temperature, reduces the tool wear, and produces the best machined surface. The machinability performance of hard turning TC4 titanium alloy on the application of air-cooling is better than the application of dry cutting process. Ren et al. [16] studied the effect of cold air and cold air with oil mist on cutting temperature, cutting force, and tool wear of Cr12 tool steel. The results show that compared with dry cutting, cold air with oil mist is the most effective cooling/lubrication condition to reduce the cutting temperature, cutting force, and tool wear of Cr12 tool steel. Brandt et al. [17] concluded through the experiment of cutting TC4 titanium alloy that low-temperature cold air can significantly improve the machining efficiency and quality and reduce the cutting temperature. Dhanchezian et al. [18] processed micro through holes on the front and rear flanks of the tool and transported liquid nitrogen to the cutting area of TC4 titanium alloy. Compared with cutting fluid cooling, the cutting temperature was reduced by about 60%, and the cutting force, surface roughness, and flank wear were reduced by more than 30%. Courbon et al. [19] carried out the experiments of liquid nitrogen-assisted cutting TC4 titanium alloy and Inconel718 nickel base superalloy, and proved the advantages of liquid nitrogen jet cooling in reducing cutting temperature and friction coefficient. Karthik et al. [20] explored the surface roughness

of SS316 under dry, wet, and low-temperature (LN2 liquid nitrogen) machining cooling methods. The results show that LN2 machining achieves better finish surface with up to 64.9%, 54.9% over dry and wet machining, respectively. Bermingham et al. [21, 22] compared liquid nitrogen cooling and dry cutting TC4 titanium alloy. The results showed that the main cutting force increased, the contact length between cuttings became shorter, the equivalent friction coefficient decreased, the shear angle increased, and the chip breaking effect was better. Chen et al. [23] developed the low-temperature nitrogen cutting supporting device and carried out the low-temperature cutting experiment of TC4 titanium alloy. Its advantages in tool wear and machined surface roughness are proved. The variation laws of cutting force and cutting temperature with machining parameters are explored. Ma et al. [24] established the empirical formula of liquid nitrogen low-temperature cutting force for 1Cr18Ni9Ti stainless steel difficult to machine materials. Chiffre et al. [25] carried out low-temperature $CO_2$ turning experiments of austenitic stainless steel. Compared with ordinary cutting fluid cooling, the machining efficiency was improved by 15 ~ 70% and the tool life was prolonged by 18 ~ 38%. Machai et al. [26] found that when cutting Ti10V2Fe3Al titanium alloy with dry ice as cooling medium, the boundary wear of the tool is reduced, the wear of the flank is relatively uniform, and the service life of the tool under high-speed conditions is prolonged by 2 times. Subsequent studies also proved the advantages of low-temperature cooling in cutting force, tool life, and chip breaking [27]. Sadik et al. [28] carried out the low-temperature cutting experiment with $CO_2$. The results show that it can inhibit the generation of tool thermal cracks and is the main factor to slow down tool wear. Jerold et al. [29] compared low-temperature cutting with liquid nitrogen and dry ice. The results show that dry ice has better cooling effect, less cutting force, better chip fracture effect, and more obvious advantages in surface roughness and tool surface wear. Qi et al. [30] carried out the experiment of low-temperature $CO_2$ cutting TC4 titanium alloy by using the internal cooling tool handle. The results show that the wear of the rear tool surface is uniform and the chip adhesion of the front tool surface is less.

In clean cutting technology, in addition to low temperature cutting technology, there are dry cutting [31–33], minimum quantity lubrication (MQL) [34–36], and enhanced minimum quantity lubrication cutting technology [37–39]. Researchers have done a lot of research on dry cutting and MQL cutting technology. When machining difficult-to-cut materials, the cooling and lubrication conditions of dry cutting are poor [7]. The lubrication conditions of MQL are improved compared to dry cutting, but the cooling capacity is still insufficient [40]. Enhanced minimum quantity lubrication technology includes nanolubricant minimum quantity lubrication (NMQL), ultrasonic vibration-assisted turning (UVAMQL), ultrasonic vibration-assisted minimum quantity lubrication (TTMQL), cryogenic minimum quantity lubrication (CMQL), and cryogenic NMQL (CNMQL). Wang et al. [37] quantitatively evaluated the cutting force, cutting temperature, tool wear, and surface quality under NMQL, CMQL, UVAMQL, and TTMQL machining conditions. The technical performance, parameter optimization, and mechanism of enhanced MQL are studied. Researchers have conducted a series of studies on enhanced micro lubrication technology. CMQL and CNMQL are the combination of low-temperature cutting technology and micro lubrication technology. Compared to MQL and NMQL, CMQL and CNMQL can improve cooling capacity. Liu et al. [38] revealed the cooling and lubrication mechanism of CMQL and its effect on material hardness, cutting force, tool wear, and surface quality of machined workpiece. Cui et al. [39] compared NMQL and CNMQL techniques by grinding TC4. As the gas phase of lubrication medium, normal temperature high-pressure air (25℃) and cryogenic high-pressure air (− 5℃) were mixed with the nanolubricant in NMQL and CNMQL, respectively. The results show that compared with NMQL and low temperature air cooling, CNMQL has the lowest grinding force, grinding peak temperature, and surface roughness.

In summary, low-temperature cutting technology and hybrid low-temperature cutting technology (CMQL, CNMQL, etc.) have obvious advantages in cutting load, surface quality, and tool wear, which can further improve machining efficiency and reduce production costs. Compared with compressor refrigeration and dry ice refrigeration, the liquid nitrogen refrigeration method can obtain lower refrigeration temperature, which provides the possibility of wider temperature control in the cutting process. At present, liquid nitrogen is mostly used directly in low-temperature cutting (− 196℃), and there is a lack of cutting data in other low-temperature ranges (18 ~ − 196℃), and the optimal cutting cooling temperature remains to be explored. In this paper, a device for mixing compressed air and liquid nitrogen is built to obtain a more stable intermediate temperature. Therefore, this provides a stable temperature condition for exploring the optimal cutting cooling temperature of materials. In addition to low-temperature machinability, the research on chip morphology evolution in the temperature ranges from 18 to − 196℃ is insufficient. Moreover, the existing low-temperature cutting research objects are mainly titanium alloy, high-temperature alloy, and high-strength alloy steel, and there is no relevant report on the impeller material FV520B. In this paper, the machinability and chip evolution of FV520B materials in different low-temperature ranges (18 ~ − 196 °C) were investigated by building a low-temperature jet cooling system. Research by Qiao et al. [41] shows that low-temperature cutting

of TC4 titanium alloy and 35CrMnSiA steel with liquid nitrogen can enhance the sawtooth degree and sawtooth pitch of chips, promote cutting fracture, and improve the machinability of materials.

In this paper, liquid nitrogen jet cooling low-temperature cutting experiments are carried out for the impeller material FV520B-hardened stainless steel, and the machinability and chip morphology are studied from the macro and micro perspectives, respectively. Based on the mixing device of liquid nitrogen and compressed air, the temperature of liquid nitrogen jet is controlled by calibrating the mixing flow. The method of controlling other physical quantities by controlling the flow rate of the fluid is also applied in other aspects. Anqi et al. [42] described the thermal management of a lithium-ion battery (LINB) cell in three dimensions. The results show that the heat transfer coefficient of lithium ion battery can be controlled by adjusting the air velocity at the inlet of air duct. A three-axis milling experiment is set up. Taking the cutting speed, axial depth, and feed per tooth as variables, the cutting force, cutting vibration, surface roughness, and tool life under different jet temperatures are measured synchronously, so as to explore the influence of low-temperature cooling on the machinability of FV520B stainless steel. The orthogonal turning experiment is set up, the cutting speed is taken as the variable, and the chip morphology, deformation degree, and adiabatic shear band under different jet temperatures are observed synchronously, so as to explore the influence of low-temperature cooling on the chip morphology evolution of FV520B stainless steel.

## 2 Experimental design

Carry out low-temperature cutting experiment for impeller material FV520B, and relevant information includes impeller material, cutting tool, machine tool, cooling system, processing parameters, and some auxiliary measurement and observation equipment.

### 2.1 Experimental materials

The workpiece material is FV520B-hardened stainless steel for impeller, and the material composition is shown in Table 1. The mechanical properties are shown in Table 2.

### 2.2 Cooling system

This paper adopts the principle of liquid nitrogen evaporation refrigeration and mixes it with compressed air to adjust the jet temperature. The low-temperature jet device adopts a self-pressurized liquid nitrogen tank to provide liquid nitrogen fluid. Air compressor provides gas fluid. Liquid nitrogen and compressed air supply pressure stable at 0.6 MPa. Throttle valve and flowmeter adjust fluid flow. Pneumatic two-piece drying filters gas water and oil. The cryogenic one-way valve prevents the backflow of gas and cryogenic fluid and is located at the front end of the gas–liquid jet mixer structure. The overall layout is shown in Fig. 1.

Firstly, the mixing ratio of liquid nitrogen and air at low temperature was calibrated. When measuring temperature, the digital thermometer probe is fixed to a position 10 mm away from the nozzle, and the flow rate of liquid nitrogen and compressed air is changed by the jet control instrument. After the jet temperature is stable, the values of liquid nitrogen flow QN2 and compressed air flow QA are recorded, as shown in Table 3. When the liquid nitrogen flow valve is closed for pure compressed air supply, the actual jet temperature is 18 °C. Due to the inevitable heat transfer throughout the equipment joints and pipelines, the jet temperature is basically stable at − 190 °C when the compressed air is closed for pure liquid nitrogen jet supply.

### 2.3 Experimental equipment and parameters

For the impeller material FV520B stainless steel, low-temperature milling experiments were carried out to explore the effects of low-temperature cooling on cutting force, cutting vibration, machined surface roughness, and tool life; At the same time, the low-temperature orthogonal turning

**Table 1** The main chemical composition of FV520B stainless steel

| Element | C | Si | Mn | Ni | Mo | Cu | Nb |
|---|---|---|---|---|---|---|---|
| Content (*wt.%*) | 0.072 ~ 0.076 | 0.28 ~ 0.36 | 13.4 ~ 13.8 | 5.48 ~ 5.62 | 1.56 | 1.58 | 0.33 |

**Table 2** FV520B material mechanical property parameters [52]

| Material | Density $\rho$/Kg/m$^3$ | Young's modulus $E$/GPa | Poisson's ratio $v$ | Yield strength $\sigma_s$/MPa | Tensile strength $R_m$/MPa | Hardness $HV$ | Section shrinkage $\Psi$ (%) |
|---|---|---|---|---|---|---|---|
| FV520B | 7800 | 210 | 0.3 | 1029 | 1078 | 300 | 61.3 |


**Fig. 1** Low-temperature jet cooling system

**Table 3** Liquid nitrogen and air flow calibration

| Temperature $T$/℃ | Flow of liquid nitrogen $QN$/m$^3$·h | Air flow $QA$/m$^3$·h |
|---|---|---|
| 18 | 0 | 1.44 |
| 0 | 0.012 | 1.44 |
| − 50 | 0.025 | 1.44 |
| − 100 | 0.032 | 1.44 |
| − 150 | 0.052 | 1.44 |
| − 190 | 0.052 | 0 |

experiment is carried out to explore the influence of low-temperature cooling on chip morphology.

#### 2.3.1 Low-temperature milling experiment

As shown in Fig. 2, the experimental machine tool is a three-axis NC machining center, and the workpiece is a cylinder with a diameter of 470 mm. The diameter of insert end milling cutter is 27 mm, and the blade material is cemented carbide. The blade is made of cemented carbide, which is produced by Zhuzhou Cemented Carbide Cutting Tools Co., Ltd., in China. Its brand is CCMT060208-HR, and model is YBM251. The rake and relief angles are 0° and 7°, respectively. The modeling and machining module of Unigraphics NX software is used to realize workpiece geometric modeling and tool path planning. YDCB-Ⅲ05 three-way piezoelectric dynamometer and DYTRAN 3035B accelerometer, combined with Coinv DASP V10 signal processing system, synchronously measure cutting force and vibration during the experiment; TR200 roughness profiler measures the roughness Ra value of the cut surface, VRM-3020F tool microscope, real-time measurement of flank wear. ISO standard is adopted, and $VB_{max} = 0.6$ mm is taken as the tool blunt standard.

The influence of low-temperature cooling on cutting force, cutting vibration, machined surface roughness, and tool life is studied by single-factor experimental method. See Table 4 for the setting of machining parameters.

#### 2.3.2 Low-temperature turning experiment

As shown in Fig. 3, the orthogonal turning experiment adopts CA6140 horizontal lathe, and the workpiece is a cylinder with a diameter of 180 mm. The blade is Mitsubishi-uncoated cemented carbide, model TPMN321, front angle 7°, back angle 11°, and no chip breaking groove. After the chips obtained by turning are treated, the chip morphology is observed by a LELCSAMEF4A metallographic microscope.

The effects of low-temperature cooling on chip morphology, chip deformation, and adiabatic shear band are studied by single-factor experimental method. The setting of processing parameters is shown in Table 5.

## 3 Results and analysis

### 3.1 Low-temperature machinability

#### 3.1.1 Low-temperature cutting force

Taking the measured three-dimensional milling force as the judgment standard, the effects of cutting speed, axial cutting depth, and feed per tooth on cutting force under different low-temperature cooling conditions are summarized and analyzed, respectively.

(1) Effect of low-temperature cutting speed on cutting force

The axial cutting depth $a_p$ is taken as 1 mm, and the feed $f_z$ of each tooth is taken as 0.1 mm/z. Change the cutting speed and jet temperature, and the change trend of cutting force is shown in Fig. 4.

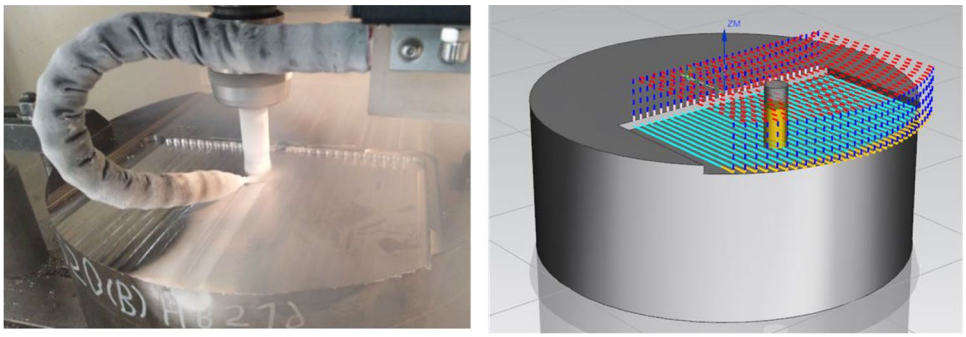

(a) Low temperature jet milling (b) Tool path

**Fig. 2** Low-temperature milling experiment, (**a**) Low temperature jet milling, (**b**) Tool path

**Table 4** Processing parameters of cryogenic milling

| Parameter | Value |
|---|---|
| Cutting speed $v$ (m/min) | 40, 80, 100, 120, 160 |
| Axial cutting depth $a_p$ (mm) | 0.5, 1, 1.5, 2 |
| Radial cutting depth (mm) | 18 |
| Feed per tooth $fz$ (mm/z) | 0.05, 0.1, 0.15, 0.2, 0.25 |
| Low temperature jet temperature $T$ (℃) | 18, 0, – 50, – 100, – 150, – 190 |


**Fig. 3** Orthogonal turning experiment at low temperature

**Table 5** Processing parameters of low-temperature turning

| Parameter | Value |
|---|---|
| Cutting speed $v$ (m/min) | 25.4, 62.2, 124.3, 254.3, 452.2, 706.5 |
| Radial cutting depth (mm) | 0.15 |
| Cutting width (mm) | 2 |
| Temperature of low temperature jet $T$ (℃) | 18, 0, – 50, – 100, – 150, – 190 |

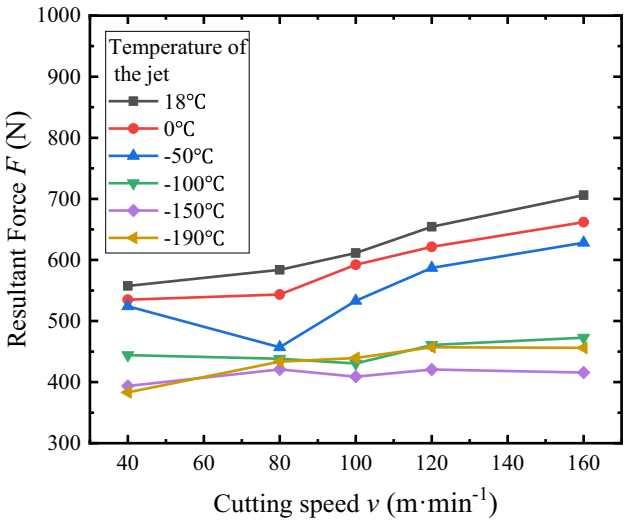


**Fig. 4** The cutting force varies with cutting speed under different low-temperature jet

As shown in Fig. 4, when the cutting speed is between 40 and 160 m/min, the cutting force decreases significantly with the decrease of jet temperature. The forced heat exchange in the cutting area by low-temperature cooling can offset the tendency of thermal softening, but it can effectively reduce the adhesion and friction between cuttings; Low-temperature cooling will also reduce the plasticity and toughness of the material, weaken the work hardening tendency, and finally reduce the cutting force. And the lower the jet temperature, the more obvious the reduction of cutting force. The corresponding cutting force values at – 100℃, – 150℃, and – 190℃ are close to each other, which is significantly less than that at 18℃, 0℃, and – 50℃. For example, the cutting force at – 100℃ is 35% lower than that at 18℃. As shown in Fig. 4, when the jet temperature is higher than – 50℃, the cutting force increases rapidly with the increase of cutting speed. However, when the jet temperature is lower than – 50℃, the cutting force almost remains

unchanged with the increase of cutting speed. This is because low temperature weakens the effect of chip friction and work hardening, which has greater advantages over strain rate strengthening and thermal softening caused by cutting speed.

(2) Influence of axial depth of low temperature cutting on cutting force

The cutting speed $v$ is 80 m/min and the feed rate $f_z$ of each tooth is 0.1 mm/z. Change the jet temperature and axial cutting depth. The change trend of cutting force is shown in Fig. 5.

As shown in Fig. 5, when the axial cutting depth is within the range of 0.5 to 2 mm, low-temperature cooling can also reduce the cutting force, and the greater the axial cutting depth, the more obvious the reduction of the cutting force, which shows that the advantages of low-temperature cooling in reducing the tendency of chip friction and work hardening under the condition of large axial cutting depth are more prominent. The cutting force corresponding to – 100℃, – 150℃, and – 190℃ decreases obviously, and the amplitude is close. When the axial cutting depth is 2 mm, the cutting force at – 100℃ is 42% lower than that at 18℃. The axial cutting depth has a linear relationship with the cutting layer area. As shown in Fig. 5, under different low-temperature jet cooling conditions, the cutting force increases linearly with the increase of axial cutting depth.

(3) Effect of feed rate per tooth on cutting force in low-temperature cutting

The cutting speed $v$ is 80 m/min and the axial cutting depth is 1 mm. Change the feed rate of each tooth and jet temperature, and the change of cutting force is shown in Fig. 6.

As shown in Fig. 6, when the feed rate of each tooth is within the range of 0.05 to 0.25 mm/z, low-temperature cooling can also reduce the cutting force, and the greater the feed rate of each tooth, the more obvious the reduction of cutting force. It also shows that large feed rate of each tooth makes the advantage of low-temperature cooling to weaken the tendency of chip friction and work hardening more prominent. The cutting force corresponding to – 100℃, – 150℃, and – 190℃ decreases obviously, and the amplitude is close. When the feed rate per tooth is 0.15 mm/r, the cutting force at – 100℃ is reduced by 52% compared with 18℃. When the feed per tooth is 0.25 mm/r, the cutting force at – 100℃ is 30% lower than that at 18℃. As shown in Fig. 6, the feed rate per tooth has a linear relationship with the cutting layer area. Under different low-temperature jet cooling conditions, the cutting force increases with the increase of feed rate per tooth; The linear relationship between cutting force and feed rate per tooth is not very significant, which is the result of low-temperature cooling and mesoscopic size effect at the same axial depth.

As shown in Figs. 4, 5 and 6, when the temperature is between 18 and – 100℃, the cutting force decreases with the decrease of temperature. This is because the low-temperature jet reduces the cutting temperature of the cutting area, which weakens the plasticity and toughness of the workpiece material. This reduces the adhesion friction between the tool and the chip and reduces the work required by the tool during the material removal process, which ultimately leads to a reduction in cutting force. When the temperature

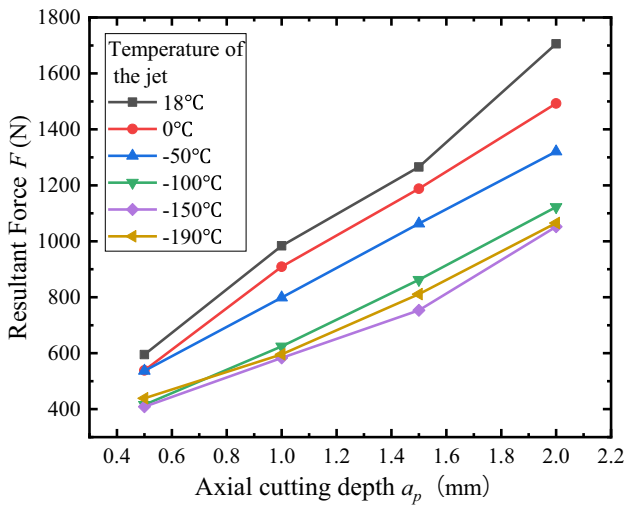


**Fig. 5** The cutting force varies with the axial depth of cut under different low-temperature jets

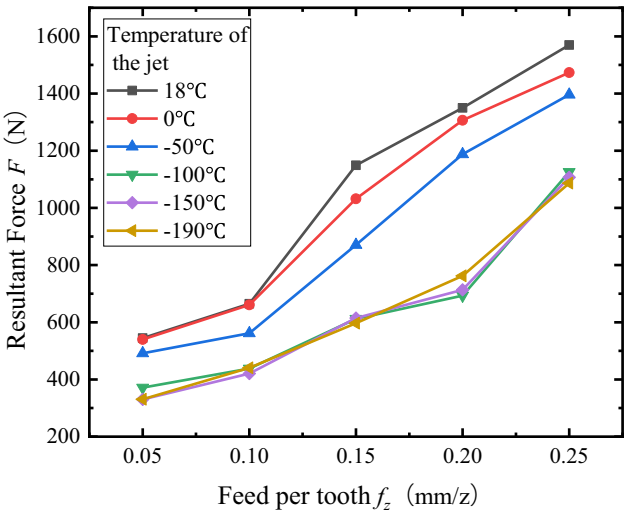


**Fig. 6** The cutting force changes with the feed of each tooth under different low-temperature jet

is between – 100 and – 190℃, the downward trend of cutting force slows down, and even the cutting force increases, which is mainly due to the sharp increase in the hardness of the workpiece material caused by the low jet temperature. Low-temperature cooling can reduce the cutting force of FV520B stainless steel. The cutting force values corresponding to the cooling conditions of – 100℃, – 150℃, and – 190℃ are very close. Therefore, from the perspective of economy and cutting force reduction, the – 100℃ cryogenic jet can replace the – 190℃ pure liquid nitrogen jet. The influence of cutting speed, axial cutting depth, and feed rate per tooth on cutting force is basically the same as that of traditional cutting.

### 3.1.2 Low-temperature cutting vibration

(1) Effect of low-temperature cutting speed on vibration

The axial cutting depth $a_p$ is 1 mm, and the feed rate $f_z$ of each tooth is 0.1 mm/z. Change the cutting speed and jet temperature, and the change of acceleration amplitude is shown in Fig. 7.

When the stiffness, natural frequency, and damping coefficient of the tool system remain unchanged, the vibration state is related to the cutting force amplitude and cutting frequency. As shown in Fig. 7, the cutting force decreases with low-temperature cooling, resulting in a decreasing trend of vibration amplitude; With the increase of cutting speed, the cutting force increases and the vibration amplitude tends to increase. The two trends are not very significant and have fluctuations, because in a specific system, when the spindle diameter is determined, the influence of cutting speed on the stability of the machining system is a lobe relationship. When cutting FV520B, the stability lobe diagram of the spindle-tool system of a specific machine tool is related to the system's characteristic parameters, flutter frequency, cutting force coefficient, etc. [43]. In the stability lobe diagram corresponding to the specific system in this paper, when the axial cutting depth and spindle diameter are unchanged, the point corresponding to the cutting speed of 40 m/min is in the unstable region above the lobe curve, and the point corresponding to the cutting speed of 80 m/min is in the stable region below the lobe curve. Therefore, when the cutting speed is lower than 80 m/min, the vibration acceleration decreases with the increase of the cutting speed. At the cutting speed of 160 m/min, the cutting vibration at – 100℃ is reduced by 37% compared with 18℃.

(2) Influence of axial depth of low-temperature cutting on vibration

The cutting speed $v$ is 80 m/min, and the feed rate $f_z$ of each tooth is 0.1 mm/z. Change the axial cutting depth and jet temperature, and the change of acceleration amplitude is shown in Fig. 8.

When the cutting frequency is fixed, the vibration state of the machining system is only related to the cutting force. As shown in Fig. 8, the amplitude of cutting vibration decreases with the decrease of jet temperature and increases with the increase of axial cutting depth. Both of them further affect the cutting vibration by changing the cutting force. The larger the cutting force, the higher the vibration amplitude. The influence trend is basically consistent with the cutting force in Fig. 5. When the axial cutting depth is 2 mm, the cut-

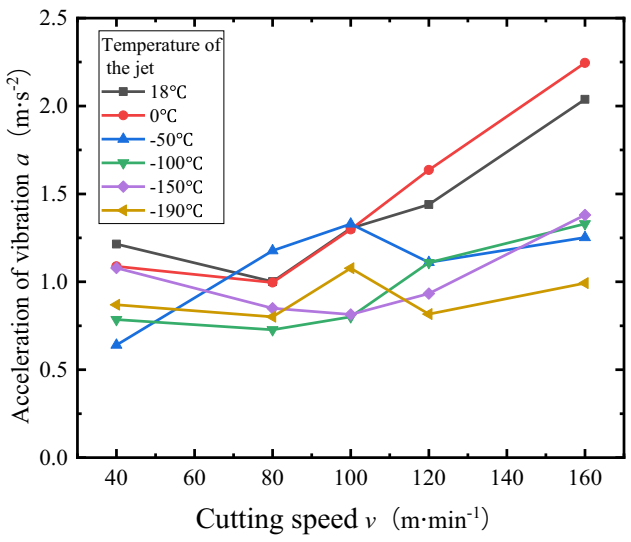


**Fig. 7** Vibration changes with cutting speed under different low-temperature jets

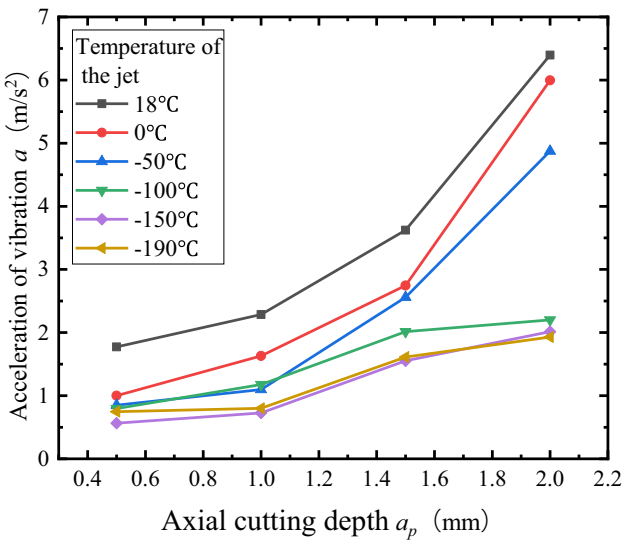


**Fig. 8** Vibration changes with axial shear depth under different low-temperature jets

ting vibration at – 100℃ is reduced by 70% compared with 18℃.

(3) Effect of feed rate per tooth on vibration in low-temperature cutting

The cutting speed $v$ is 80 m/min and the axial cutting depth $a_p$ is 1 mm. Change the feed rate of each tooth and jet temperature, and the change of acceleration amplitude is shown in Fig. 9.

As shown in Fig. 9, the amplitude of cutting vibration decreases with the decrease of jet temperature and increases with the increase of feed per tooth. They also further affect the cutting vibration by changing the cutting force, and the influence trend is also directly related to the change of cutting force in Fig. 6. When the feed rate per tooth is 0.25 mm/z, the cutting vibration at – 100℃ is reduced by 62% compared with 18℃.

In conclusion, low-temperature cutting FV520B stainless steel can improve the stability of the processing system. Axial cutting depth, jet temperature, and feed rate per tooth affect cutting vibration by changing cutting force. Cutting speed affects cutting vibration by changing cutting force and cutting frequency. The vibration amplitude corresponding to the cooling conditions of – 100℃, – 150℃, and – 190℃ is close. From the point of view of reducing cutting vibration and economy, – 100℃ jet can replace pure liquid nitrogen jet.

#### 3.1.3 Surface roughness under low-temperature cutting conditions

(1) Effect of cutting speed on surface roughness at low temperature

The axial cutting depth $a_p$ is taken as 1 mm, the feed rate $f_z$ of each tooth is taken as 0.1 mm/z, the roughness of the cut surface is taken as the average value after three measurements, and the cutting speed and jet temperature are changed. The change of surface roughness is shown in Fig. 10.

As shown in Fig. 10, low-temperature cooling can significantly reduce the surface roughness value of the cut surface. When the jet temperature is 18℃ and 0℃, the surface roughness value of the workpiece first increases with the increase of the cutting speed, and then decreases with the increase of the cutting speed. This is due to the formation of chip buildup, which leads to the increase of the machined surface roughness of the workpiece. As shown in Fig. 11, when $v = 100$ m/min, the machined surface topography of the workpiece under different low temperature jets. When the temperature is 18℃ and 0℃, there are pits and other defects on the surface, which just proves this conclusion. Proper temperature and pressure are required for the formation of chip buildup. When the cutting speed exceeds 100 m/min, the sliding resistance and friction coefficient of the chip bottom layer decrease significantly due to the high cutting temperature. At this time, the chip buildup disappears, resulting in the reduction of the workpiece surface roughness. When the jet temperature is lower than – 50℃, the relationship between the surface roughness and the cutting speed is not signifi-

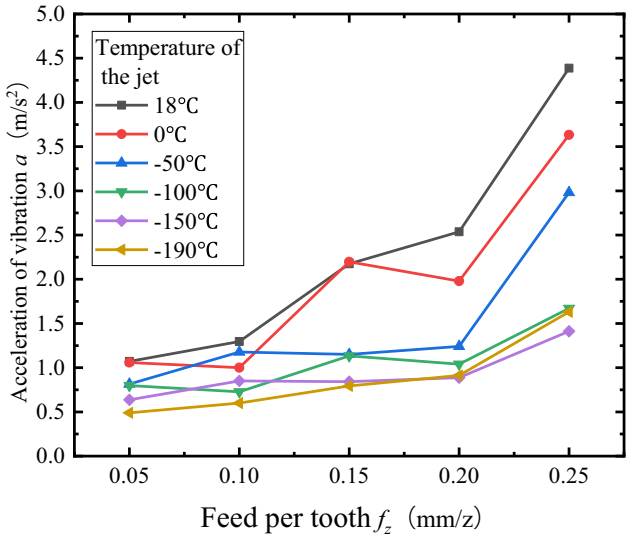


**Fig. 9** Vibration changes with the feed of each tooth under different low-temperature efflux

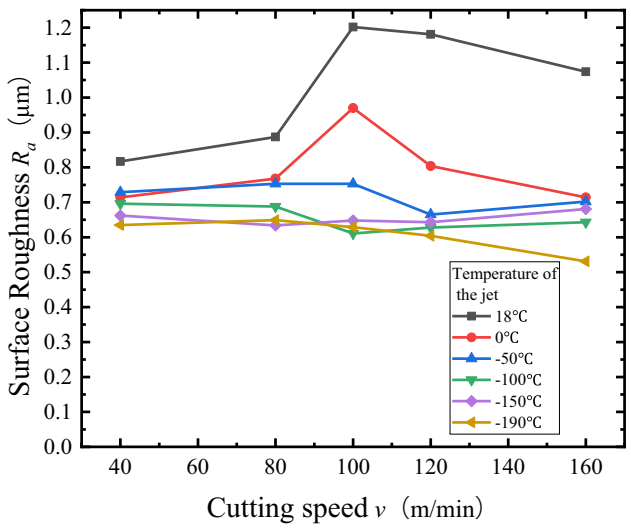


**Fig. 10** Changes of surface roughness with cutting speed under different low-temperature jets

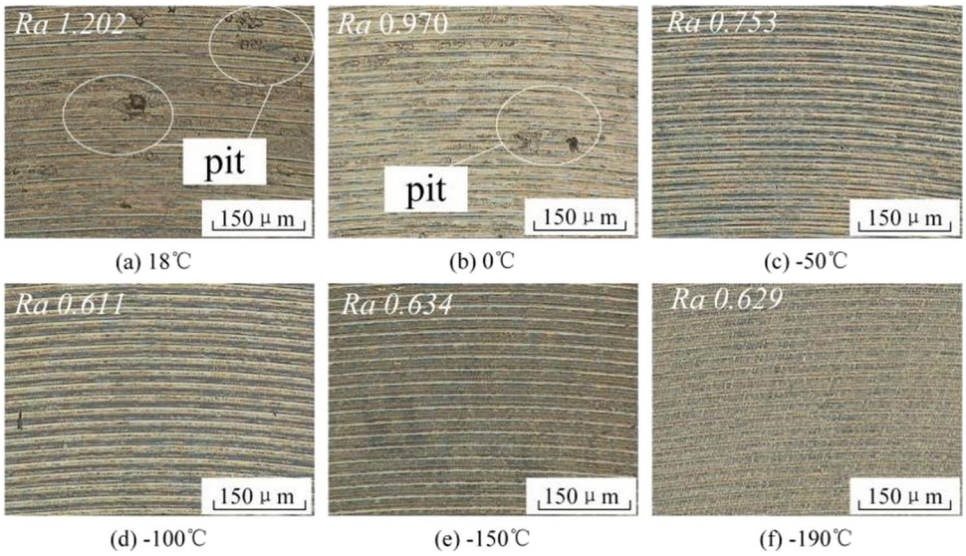


**Fig. 11** When $v = 100$ m/min, the morphology of the processed surface of the workpiece under different low-temperature jets

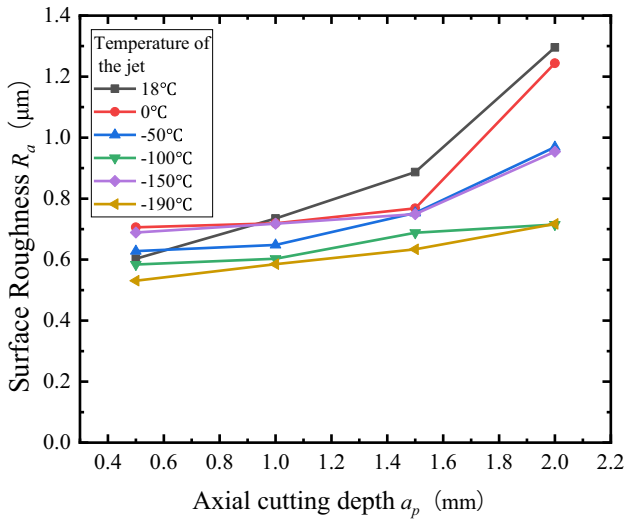


**Fig. 12** Changes of surface roughness with axial shear depth under different low-temperature jets

cant. This is because the lower cooling temperature can effectively prevent the chip from sticking to the tool tip and avoid the generation of chip buildup. And the low temperature jet reduces the plasticity of the workpiece material. This leads to the reduction of the ploughing effect of the blunt radius and the rear blade surface on the machined surface. Therefore, the surface roughness is generally reduced below – 50℃.

(2) Effect of cutting axial depth on surface roughness at low temperature

The cutting speed $v$ is 80 m/min, the feed rate $f_z$ of each tooth is 0.1 mm/z, the axial cutting depth and jet temperature are changed, and the change of surface roughness is shown in Fig. 12.

As shown in Fig. 12, the increase of surface roughness under the condition of small axial cutting depth is not obvious. When the axial cutting depth exceeds 1.5 mm, the surface roughness increases obviously, especially at 18℃ and 0℃. The reason is that the thermal load of cutting force under small axial cutting depth is small, and the plastic deformation of the material is not obvious. With the increase of axial cutting depth, the thermal load becomes larger, and the plastic deformation leads to the aggravation of the deterioration of the machined surface. As shown in Fig. 12, under the same axial cutting depth, the surface roughness is significantly improved with the decrease of jet temperature. The reason is that low-temperature cooling effectively reduces the thermal load of cutting force and reduces the elastic–plastic properties of materials, resulting in the reduction of the contact surface between the tool flank and the cutting surface and the improvement of surface quality. When the axial cutting depth is large, the cooling effect of low temperature on the cutting area and the modification effect on the material are more and more obvious. The surface roughness values corresponding to – 150℃ and – 190℃ are close, which is reduced by 45% compared with normal temperature and 0℃.

(3) Effect of feed rate per tooth on surface roughness in low temperature cutting

The cutting speed $v$ is 80 m/min and the axial cutting depth $a_p$ is 1 mm. Change the feed rate of each tooth and jet temperature. The change of surface roughness is shown in Fig. 13.

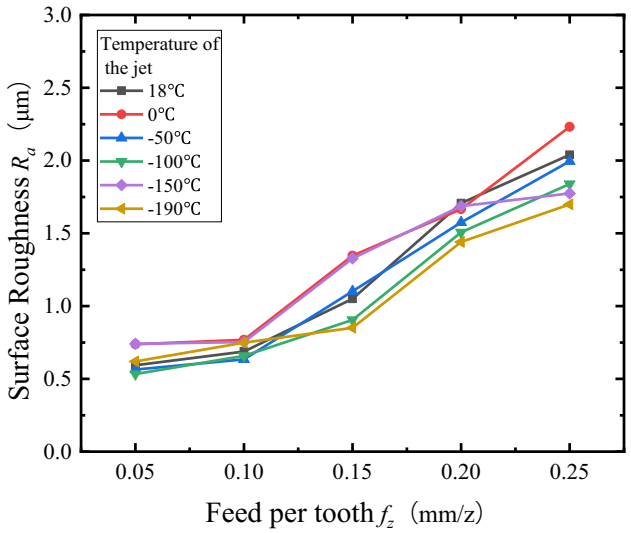


**Fig. 13** Surface roughness changes with the feed rate of each tooth under different low-temperature efflux

Compared with the plastic deformation of materials, the geometric residual height of the cutting surface has a more significant effect on the surface roughness. The feed per tooth is directly related to the feed rate, which directly determines the distance between the tool marks and the tool marks on the machined surface. As shown in Figs. 13 and 14, when the feed per tooth increases, the surface roughness increases obviously. When the feed rate of each tooth is small, the influence of geometric factors is weak, and the increase of roughness is not significant. When it is greater than 0.1 mm/z, the roughness value increases linearly. Although the feed rate per tooth is the primary factor causing the change of surface roughness, low temperature can reduce the cutting force, thermal load, and material elastoplasticity, and also improve the surface roughness. When the feed rate of each tooth is 0.25 mm/z, compared with the surface roughness under normal temperature cutting, the surface roughness values of low-temperature cutting at – 100℃, – 150℃, and – 190℃ are reduced by 18%, 21%, and 23%, respectively.

To sum up, low-temperature cutting FV520B-hardened stainless steel can reduce the cutting load, material elastoplasticity, and surface roughness at the same time. The cutting speed and axial cutting depth are the physical factors affecting the surface roughness, and the feed rate per tooth is the geometric factor affecting the surface roughness. From the point of view of economy and surface roughness, – 100℃ jet can replace pure liquid nitrogen jet.

#### 3.1.4 Tool life under low-temperature cutting conditions

(1) Trend of tool wear in low temperature cutting

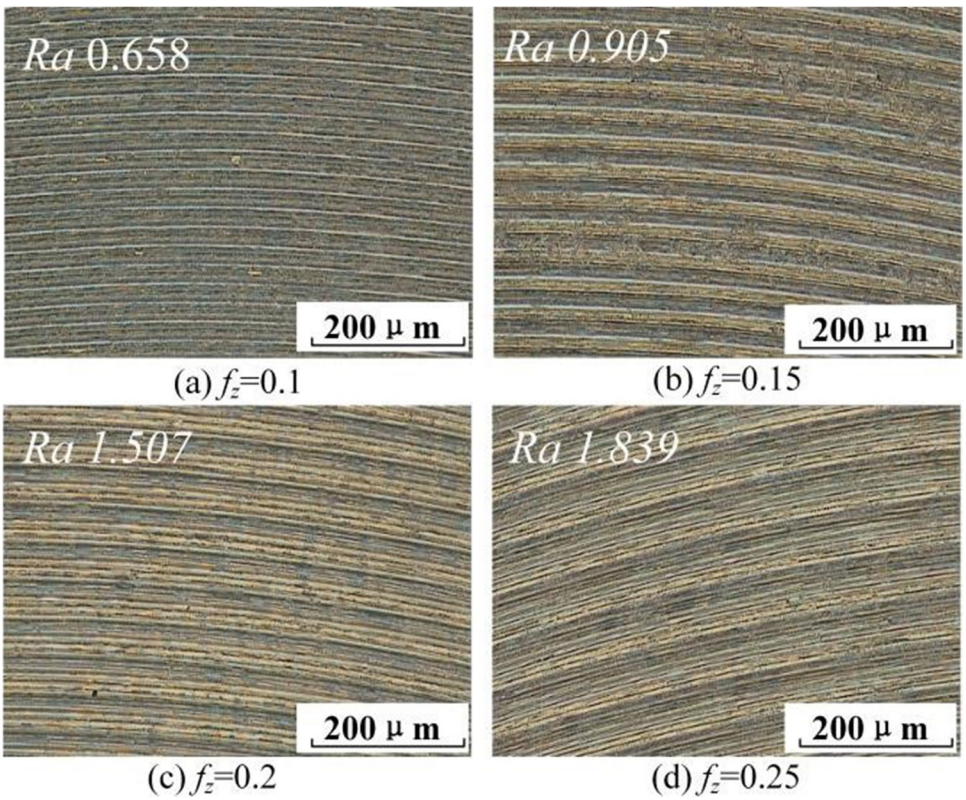


**Fig. 14** The influence of the change of feed per tooth on the machined surface morphology under the condition of low-temperature jet flow at – 100℃

**Table 6** Tool life under different cooling conditions

| Temperature of the jet $T$ (℃) | Amount of flank wear $VB$ (mm) | | | | | | | | |
|---|---|---|---|---|---|---|---|---|---|
| | 2.5 min | 5 min | 10 min | 15 min | 20 min | 25 min | 30 min | 35 min | 40 min |
| 18 | 0.102 | 0.203 | 0.29 | 0.314 | 0.406 | Breaking | | | |
| 0 | 0.11 | 0.198 | 0.262 | 0.295 | 0.386 | Breaking | | | |
| − 50 | 0.113 | 0.213 | 0.25 | 0.285 | 0.314 | 0.433 | Breaking | | |
| − 100 | 0.105 | 0.166 | 0.208 | 0.231 | 0.298 | 0.369 | 0.479 | 0.621 | Abate |
| − 150 | 0.108 | 0.172 | 0.197 | 0.229 | 0.305 | 0.388 | 0.456 | 0.608 | Abate |
| − 190 | 0.085 | 0.159 | 0.172 | 0.235 | 0.311 | 0.374 | 0.469 | 0.594 | Breaking |

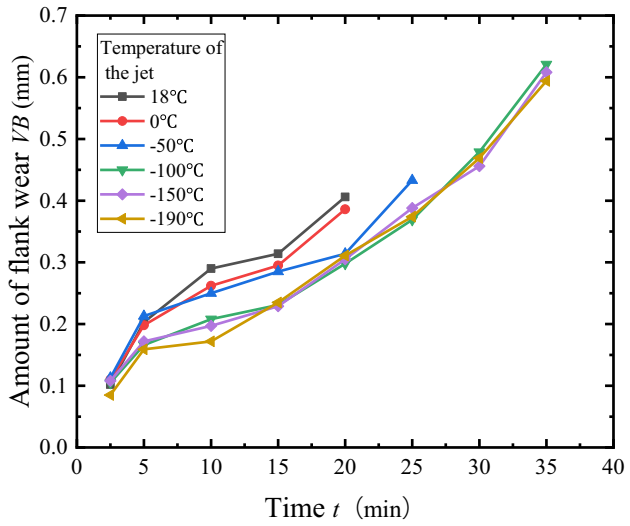


**Fig. 15** Rear tool surface wear curve of low-temperature cutting tool

The cutting speed $v$ is 80 m/min, the axial cutting depth $a_p$ is 1 mm, and the feed rate of each tooth is 0.1 mm/z. Change the jet temperature, and the wear amount during the tool life is shown in Table 6. Under the conditions of 18℃, 0℃, − 50℃, and − 190℃ jet, the tool is damaged and invalid, and the service life is 25 min, 25 min, 30 min, and 40 min, respectively; Under the condition of − 100℃ and − 150℃ jet, the normal wear failure of the tool occurs, and the service life is 35 min. In general, low-temperature cutting prolongs the tool life, and the tool life corresponding to − 100℃ is 43% higher than that at room temperature.

According to the data in Table 6, the tool life curves under different low-temperature conditions are obtained, as shown in Fig. 15. The overall trend conforms to the three-stage process of initial wear, normal wear, and sharp wear. In the normal wear stage, low temperature cooling can significantly reduce tool wear and prolong tool life. The tool life under the cooling conditions of − 100℃, − 150℃, and − 190℃ is close, but the liquid nitrogen cooling under the condition of − 190℃ reduces the mechanical properties of the tool material, and finally leads to edge collapse. Therefore, − 100℃ and − 150℃ jet can be used to replace pure liquid nitrogen cooling.

Figure 16-(a) and-(b) correspond to the tool wear at different time nodes under cooling conditions of 18℃ and − 190℃, respectively. The results show that low temperature can effectively slow down the tool failure process. Liquid nitrogen cryogenic cooling can not only reduce the cutting force, but also accelerate the heat transfer between the outside world and the tool, workpiece, and chip. The element diffusion and bonding in the contact area can be curbed by reducing the temperature, pressure, and thermopower of the tool-chip and tool-work contact areas, and finally, the tool wear can be reduced. At the same time, low-temperature cooling will reduce the elastic–plastic material, reduce the contact length between tool and chip, tool, and workpiece, and further reduce the possibility of contact surface bonding. In addition, liquid nitrogen gasification partially isolates the cutting area and prevents the contact surface from chemically reacting with air and corroding the tool. The mechanism of tool damage is different between 18 and − 190℃ cooling conditions. In Fig. 16-(a)-(4), chip is attached to the broken part of the cutting edge of the tool. At this time, the temperature and pressure in the cutting area of the workpiece are higher, the deformation speed of the workpiece material in the contact surface is fast, and the yield strength is obviously improved. The yield strength of the tool material decreases due to high temperature, and the plastic damage occurs when the cutting edge is blunted to a certain extent. In Fig. 16-(b)-(4), the cutting edge of the cutting tool under the condition of − 190℃ jet flow is very smooth. Under discontinuous cutting conditions, the cutting edge is affected by alternating mechanical stress and alternating thermal stress caused by cooling. With the increase of load cycles, the crack in the cutting edge becomes unstable and expands, leading to brittle damage.

The left side of Fig. 17 (a) and (b) are the SEM photos of the flank wear area of the blade at 18℃ and − 190℃, respectively. The cutting time is 20 min. The right side of each picture is the EDS scanning energy spectrum analysis of the red box area in the corresponding left picture. The instrument

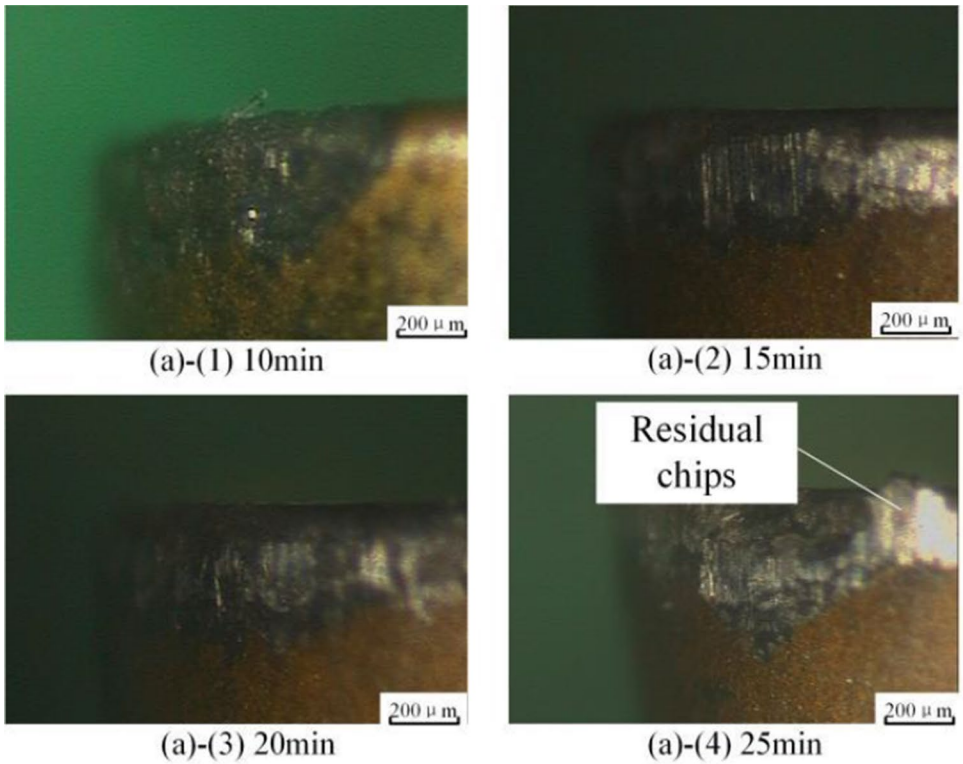


（a）The flank wear morphology at 18℃

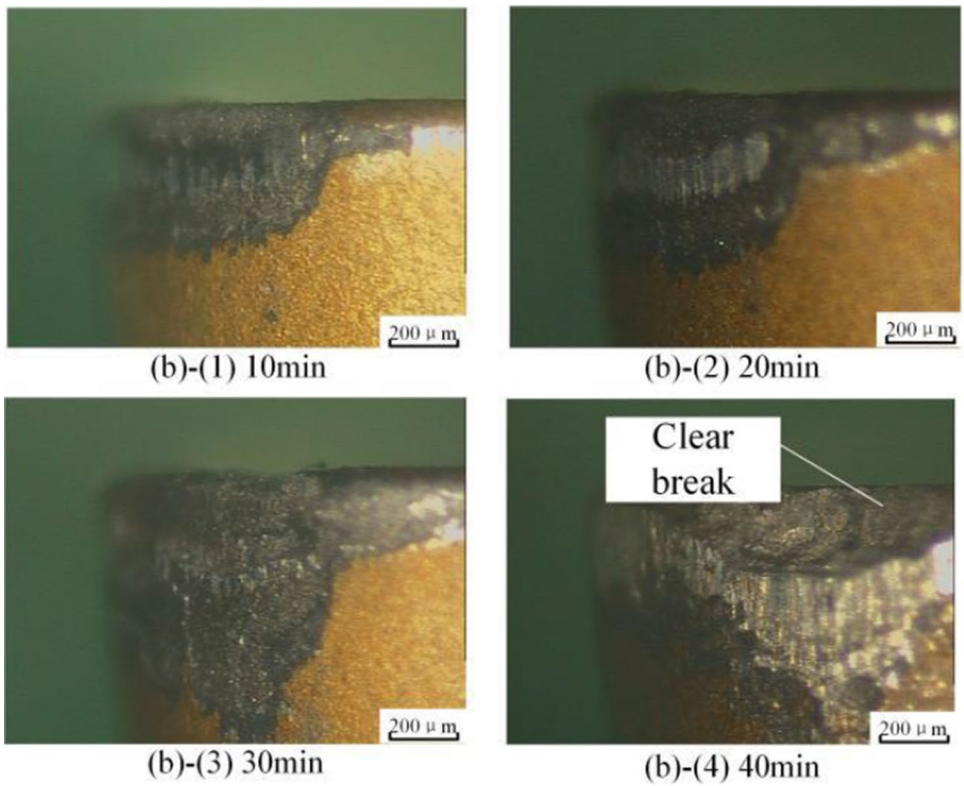


（b）Wear morphology of flank face at -190℃

**Fig. 16** Process of tool surface wear at 18℃/ − 190℃

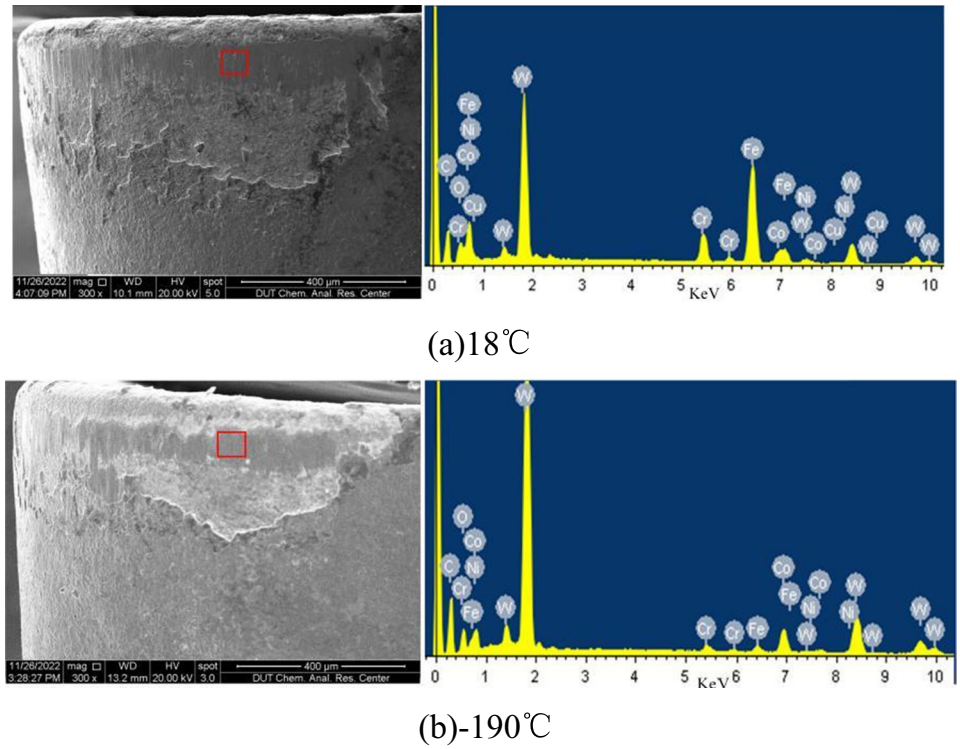


**Fig. 17** Tool wear morphology and energy spectrum analysis at 18 °C and – 190 °C

adopts the tungsten filament scanning electron microscope produced by FEI company, model QUANTA 45,003,040,702. The blade material is based on cemented carbide and contains C, Co, W, and other elements. There are TiCN, $AlO_3$, and TiN coatings outside the substrate, so it also contains Ti, N, Al, and O elements. It can be seen from Table 1 that the elements contained in the material FV520B include Mn, Ni, Mo, Cu, Nb, and other elements in addition to Fe. According to the EDS analysis in Fig. 17, it is obvious that more Fe, Ni, Cu, and other elements of the workpiece diffuse into the tool surface at 18℃ compared with – 190℃. This verifies the hindering effect of low-temperature cutting conditions on tool diffusion wear.

## 3.2 Chip morphology evolution under low-temperature cutting conditions

The essence of cutting is the process of material cutting layer transforming into chip through plastic shear. In order to further reveal the influence of low-temperature cooling on the cutting process from the microscopic point of view, a series of low temperature orthogonal turning experiments were set up to study the chip morphology evolution under different low-temperature jets (– 190–18℃) and cutting speeds.

### 3.2.1 Chip topography under low-temperature cutting conditions

The experimental parameters are shown in Table 4. In the experiment, the cutting speed and cooling jet temperature were changed, and then the chips were collected, fixed, ground, polished, and corroded. The chip morphology under the metallographic microscope is shown in Figs. 18, 19, 20, 21, 22 and 23.

As shown in Figs. 18, 19, 20, 21, 22 and 23, the impeller material FV520B under different jet temperature conditions, with the increase of cutting speed, its chip changes from banded to serrated, and the degree of serration gradually increases. Taking the chip under 0℃ low-temperature cutting condition as an example, Fig. 19-(a) shows the banded chip with uniform plastic deformation; Fig. 19-(c) is serrated chip; serrated shape is uneven; with the further increase of cutting speed, Fig. 19-(d) is uniform-serrated chip. Chips are formed in the shear plane, and the deformation rate of the shear zone corresponding to high cutting speed is on the order of 103–104 [44]. When the thermal softening caused by high speed and large strain is dominant over strain hardening and strain rate strengthening, adiabatic shear bands appear.

Jet temperature has a significant effect on chip evolution. The decrease of temperature is more conducive to the formation of adiabatic shear bands. The serrated spacing and serrated degree of chips increase significantly with the decrease of jet temperature, and the critical cutting speed of adiabatic shear decreases. Taking the chip under the cutting speed of 124.3 m/min as an example, as shown in Fig. 19-(c), the serrated chip under low-temperature cutting at 0℃ has a deformation band, while the serrated chip under low-temperature cutting at – 190℃ in Fig. 19-(c) has a narrow

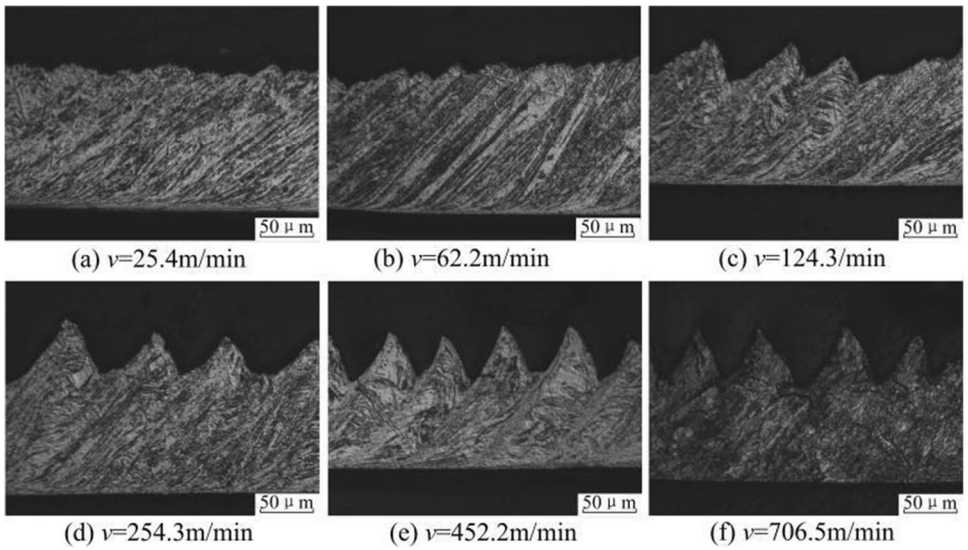


**Fig. 18** Chip morphology during cutting at a jet low temperature of 18℃

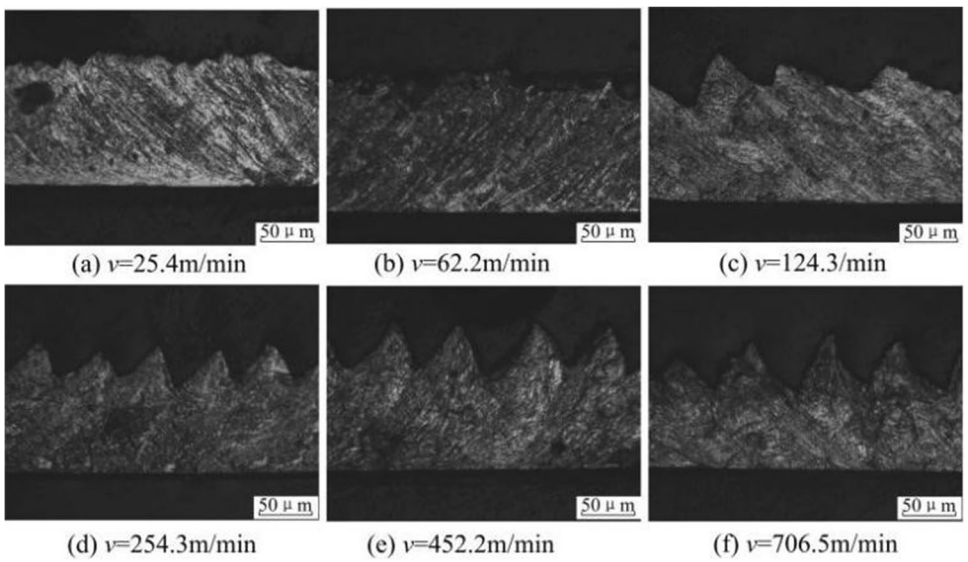


**Fig. 19** Chip morphology during cutting at a jet low temperature of 0℃

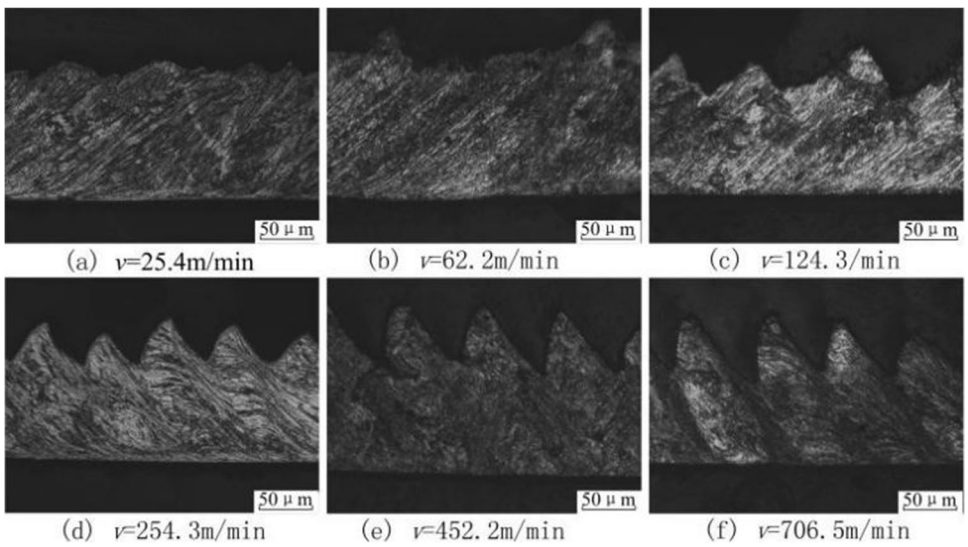


**Fig. 20** Chip morphology during cutting at a jet low temperature of − 50℃

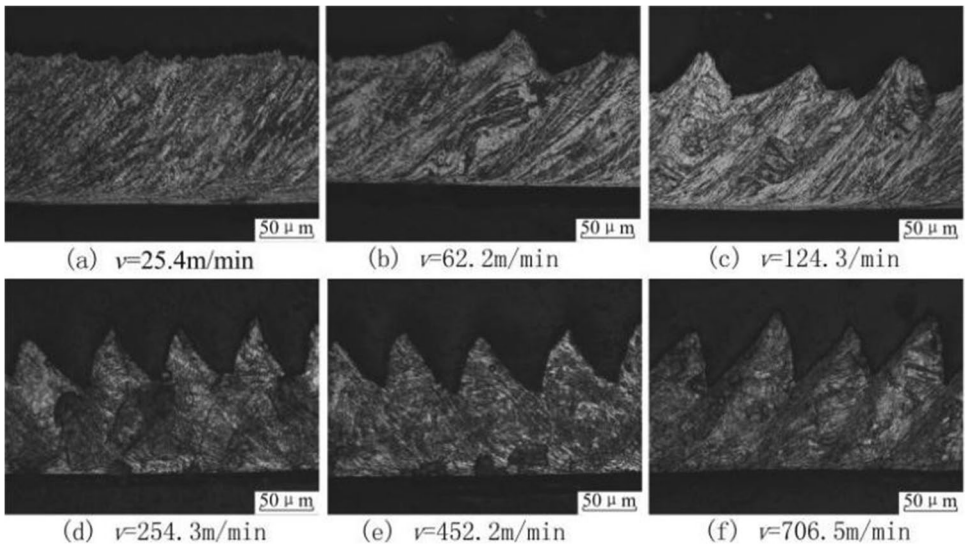


**Fig. 21** Chip morphology during cutting at a jet low temperature of – 100℃

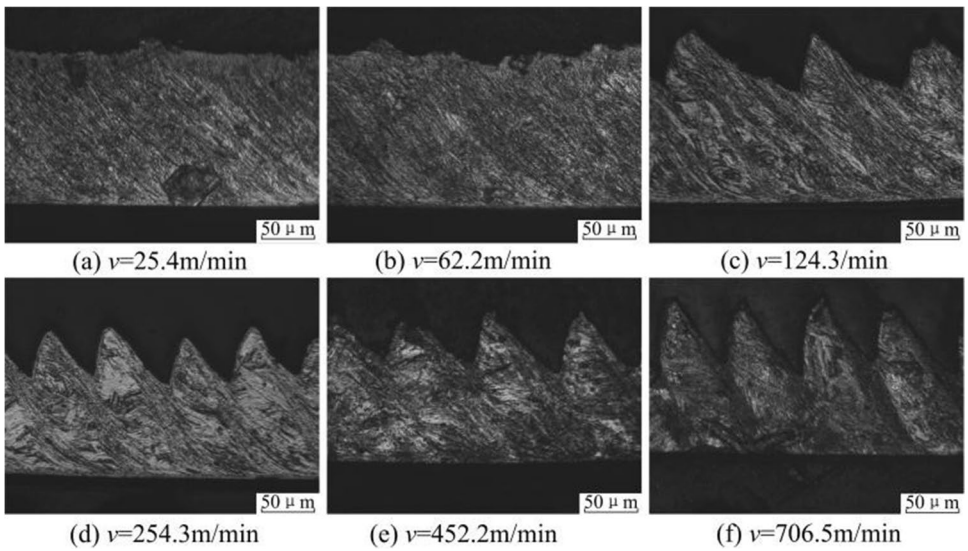


**Fig. 22** Chip morphology during cutting at a jet low temperature of – 150℃

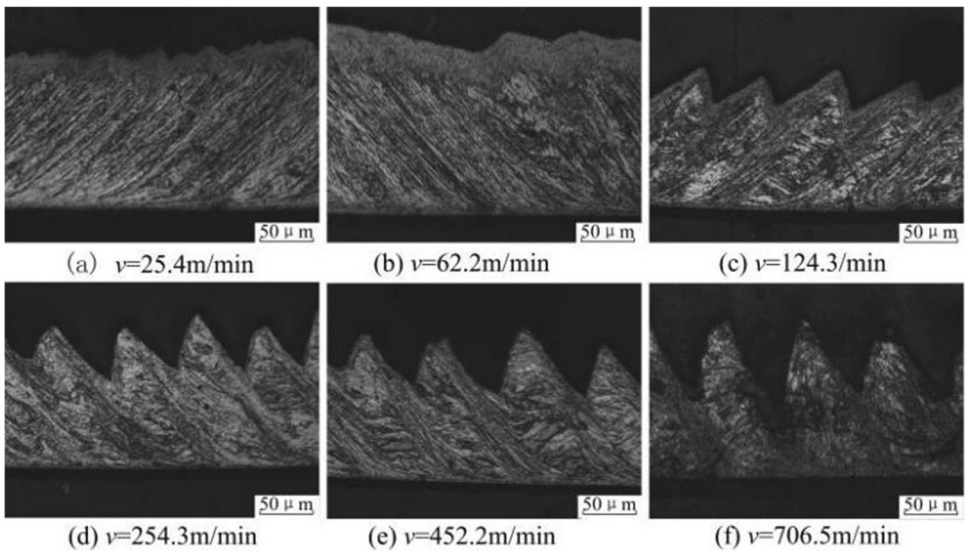


**Fig. 23** Chip morphology during cutting at a jet low temperature of – 190℃

transition band. The low-temperature jet cooling makes the impeller material show hard brittle effect, which leads to the increase of compressive stress in the shear zone [45] and promotes the formation of shear band.

### 3.2.2 Low-temperature cutting chip deformation characterization

(1) Chip deformation coefficient

Chip deformation coefficient $\xi$ is an important parameter to measure the plastic deformation of cutting layer, which represents the thickness ratio between chip layer and cutting layer. As shown in Fig. 24, the thickness of a serrated chip takes the average of the peak tooth height $H$ and the valley tooth height $h$. Change the cutting speed and jet temperature; chip deformation coefficient results are shown in Fig. 25.

The chip deformation coefficient decreases rapidly with the increase of cutting speed, and decreases slightly with the decrease of cooling temperature. Uniform plastic accumulation occurs inside the strip chip, the thickness is greater than the cutting layer, and the deformation coefficient is greater than 1; the plastic deformation of serrated chip mainly occurs in adiabatic shear band, and the deformation coefficient is less than 1. The low temperature has a decreasing effect on the thermal load of cutting force and the plastic mechanical properties of impeller material. The combined effect of the two aspects leads to the deformation coefficient less than that of normal temperature cutting.

(2) Degree of chip serration

In order to further describe the plastic deformation degree of serrated chips, the ratio of tooth height $H-h$ to tip height $H$ is defined as the serrated degree $Gs$. Changing the cutting speed and jet temperature, the measurement results of chip serration degree are shown in Fig. 26. The serration degree of 0 represents the banded chip.

When the cutting speed is low, the serration degree of the chip increases rapidly. When the critical speed is reached, the serration degree increases slowly and approaches 1, and finally fracture occurs. When the cutting speed is constant, the degree of chip serration increases with the decrease of the jet temperature. The reason is that the low-temperature cooling reduces the plasticity of the impeller material and increases the hardness.

(3) Chip pitch

As shown in Fig. 24, the chip pitch $L_p$ refers to the distance between adjacent teeth. After changing

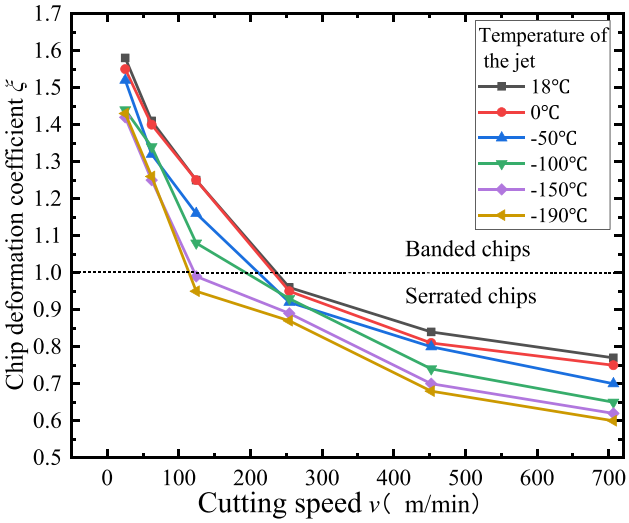


**Fig. 25** Chip deformation coefficient during low-temperature cutting

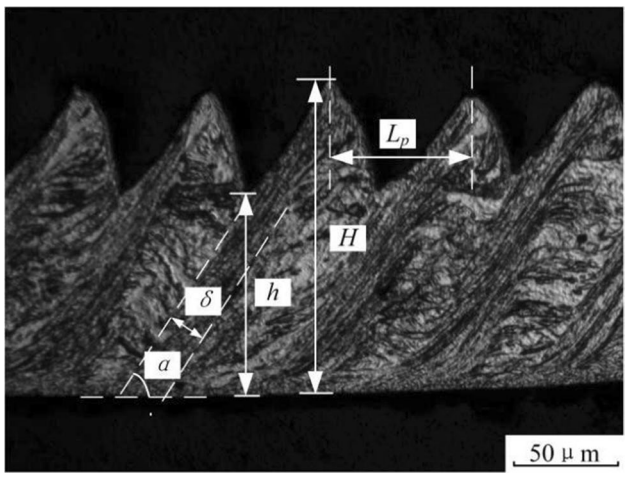


**Fig. 24** Geometry of sawtooth chips

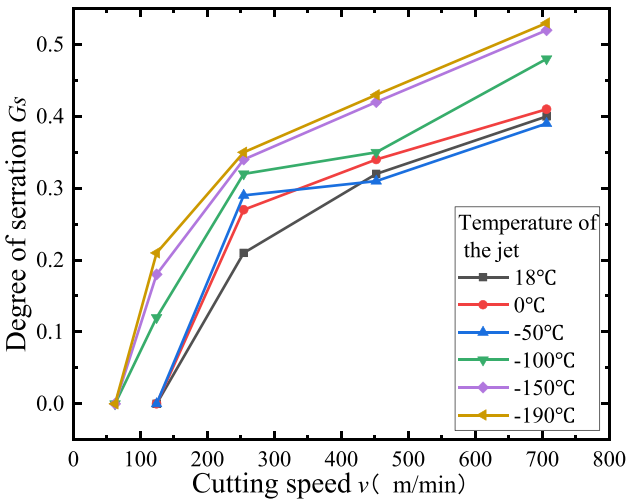


**Fig. 26** Serration degree of chip during low temperature cutting

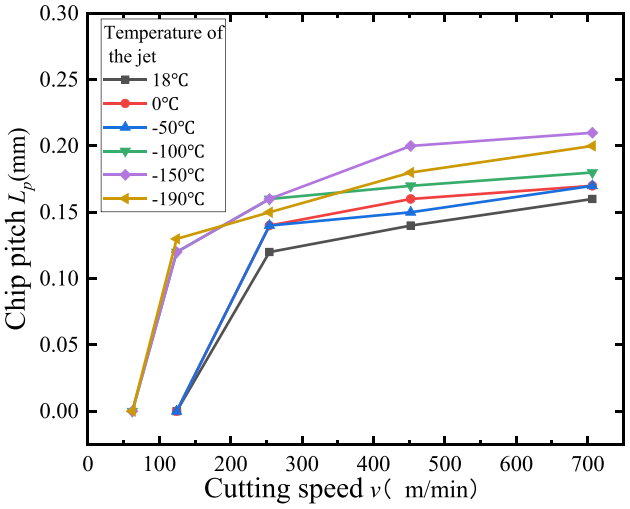


**Fig. 27** Chip pitch during low temperature cutting

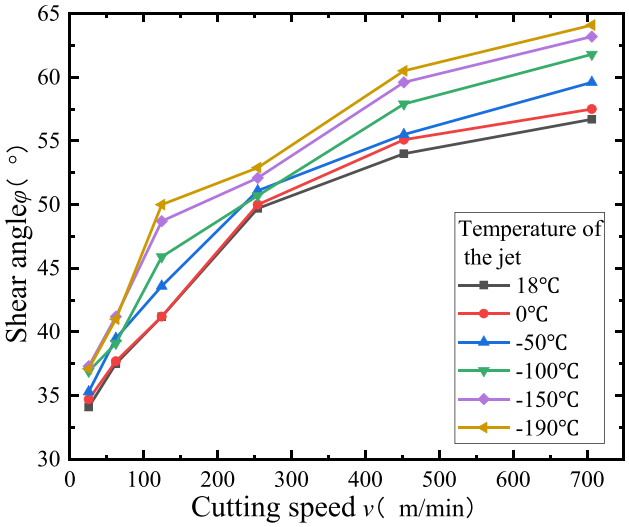


**Fig. 28** Chip shear angle during low-temperature cutting

the cutting speed and jet temperature, the chip pitch measurement results are shown in Fig. 27. After the cutting speed reaches the critical value, the chip pitch does not change significantly with the cutting speed, but increases significantly with the decrease of the jet temperature. Although the increase of cutting speed increases the strain rate, the process of chip energy accumulation will also accelerate simultaneously. Therefore, the influence of cutting speed on pitch is limited. The influence of low temperature on the pitch mainly includes reducing the plastic flow performance of the material, increasing the hardness of the material, increasing the energy threshold of adiabatic shear during cutting, and increasing the moving distance of the tool along the feed direction during the energy accumulation process.

(4) Shear angle

Shear angle $\phi$ is an important parameter of the first deformation zone. After changing the cutting speed and jet temperature, cutting chip pitch measurement results are shown in Fig. 28. With the increase of cutting speed, the shear angle increases rapidly, when the serrated chip time-varying rate gradually flatten. As the cooling temperature decreases, the shear angle decreases. When the cutting speed is higher, the effect of low temperature is more obvious. The shear angle is inversely related to the chip deformation coefficient [46], and the trend of the shear angle calculated according to Fig. 25 is consistent with the results of Fig. 28. In addition, when the rake angle is constant, the shear angle is inversely related to the friction coefficient [47], and the low temperature can effectively reduce the friction coefficient between the chips. It can also be concluded that the shear angle increases with the decrease of temperature.

### 3.2.3 Adiabatic shear bands under low-temperature cutting conditions

(1) Width of adiabatic shear band

As shown in Fig. 24, the adiabatic shear band is the prerequisite for the formation of serrated chips, and its width $\delta$ is a key indicator for measuring serrated chips. Changing the cutting speed and jet temperature, the width of the adiabatic shear band obtained by the turning experiment is shown in Fig. 29. Impeller material with high strength, low thermal conductivity, high shear surface cutting temperature, high-speed cutting shear in-plane strain rate. This causes the shear adiabatic shear band width to gradually narrow. When the cutting speed increases to a certain extent, the strain rate of the shear plane approaches the limit, and the narrowing rate of the shear band width slows down. Continue to increase the cutting speed; micro holes and cracks gradually appear in the adiabatic shear band, eventually leading to chip fracture. As shown in Fig. 29, low temperature has a significant effect on the width of the adiabatic shear band. The lower the cooling temperature, the narrower the adiabatic shear band. The effect of low temperature on reducing the width of the adiabatic shear band is consistent with the trend of promoting serrated chip formation. Low-temperature cooling makes the mechanical properties of the material have a hard and brittle tendency [48, 49], and the plastic flow of the metal is weakened. When the cutting heat in the shear zone is concentrated to a certain extent, the large

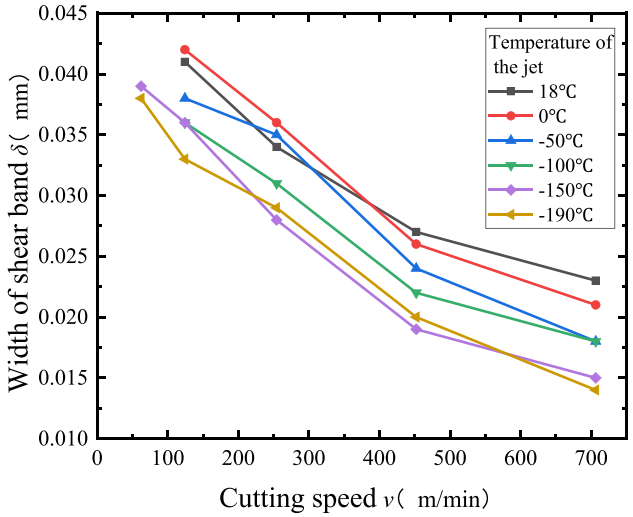


**Fig. 29** The adiabatic shear band width of chips during low-temperature cutting

strain rate of high-speed cutting makes the material of the shear surface attachment less than plastic deformation, which eventually leads to the adiabatic shear band narrowing.

A large number of experiments show that the serrated chips obtained under low-temperature cutting are similar to those obtained under room temperature cutting, and the adiabatic shear bands also include deformation bands and transition bands [50, 51]. As shown in Fig. 30-(a), plastic deformation occurs in a wide area centered on the shear plane to form a deformation band, and the grains are fibrotic under the combined action of force and heat; as shown in Fig. 30-(b), as the cooling temperature decreases, plastic deformation occurs in a narrow region centered at the shear plane to form a transition band.

(2) Angle of adiabatic shear band

As shown in Fig. 24, the adiabatic shear band inclination angle $\alpha$ is also one of the parameters describing the serrated chip. Changing the cutting speed and jet temperature, the adiabatic shear band inclination angle obtained by the turning experiment is shown in Fig. 30. The inclination angle of adiabatic shear band decreases with the decrease of cooling temperature, and has an inverse linear relationship with cutting speed. Under the premise of a certain rake angle of the cutting tool, the sum of the shear angle and the inclination angle of the shear band is a fixed value, and the trend of Fig. 31 is inversely related to the trend of Fig. 28.

## 4 Conclusion

In this paper, the liquid nitrogen-compressed air mixed low temperature cutting experiment was carried out for the hardened stainless steel FV520 B used in the impeller.

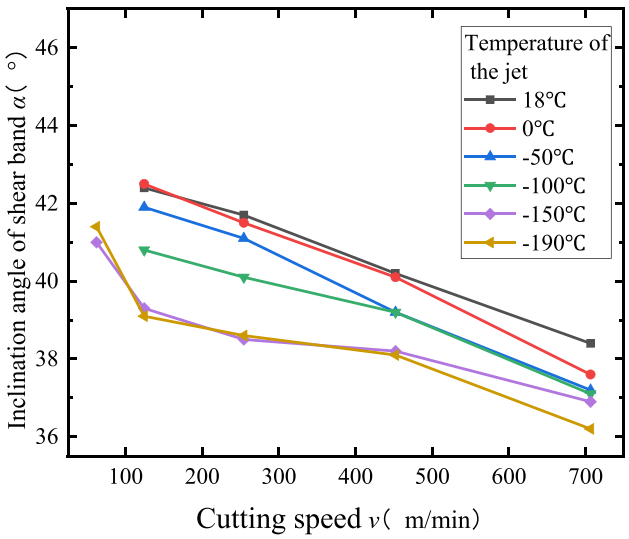


**Fig. 31** Dip angle of adiabatic shear band of chips during low-temperature cutting

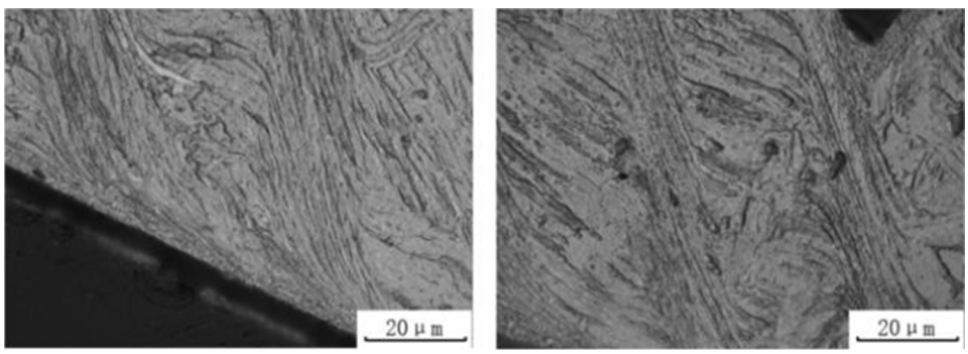


(a) Deformation band (b) Transition zone

**Fig. 30** Cutting adiabatic shear band at low temperature, (**a**) Deformation band, (**b**)Transition zone

The low-temperature machinability and chip morphology evolution at different jet temperatures were studied. The results show that low temperature cooling can significantly improve the machinability and chip breaking effect of materials. The main conclusions are as follows:

(1) The experiments of low-temperature milling FV520B show that low-temperature cooling can effectively reduce cutting force, vibration, and surface roughness. When the cutting speed is 80 m/min, the axial cutting depth is 1 mm, and the feed per tooth is 0.25 mm/r; the cutting force, cutting vibration, and workpiece surface roughness at − 100℃ are reduced by 30%, 62%, and 18% respectively compared with 18℃. With the increase of cutting speed, feed per tooth, and axial cutting depth, the improvement effect of low temperature is more obvious. When the cutting speed is 80 m/min, the feed per tooth is 0.1 mm/r, and the axial cutting depth is 0.5 mm; the cutting force at − 100℃ is 200 N lower than that at 18℃. Under the same cutting speed and feed per tooth, when the axial cutting depth is 2 mm, the value is 550 N.
(2) Low-temperature cooling can prolong tool life; when the cutting speed is 80 m/min, the axial cutting depth is 1 mm, and the feed per tooth is 0.1 mm/z; the tool life at − 100℃ is 43% higher than that at room temperature. Compared with the plastic damage of normal temperature cutting, the failure mode of low temperature cutting tool is mainly brittle chipping. When the jet temperature is reduced to below − 100℃, the improvement effect of machinability is approximately the same.
(3) The low-temperature turning experiment of FV520B-hardened stainless steel shows that when the cutting speed increases, the chip gradually changes from banded to serrated; the deformation coefficient and the inclination angle of the adiabatic shear band decrease; the serration degree, pitch, and shear angle increase; and the adiabatic shear band narrows. When the cooling temperature decreases, the chip deformation coefficient and the inclination angle of the adiabatic shear band decrease; the degree of serration, pitch, and shear angle increase; the adiabatic shear band narrows; and the critical cutting speed issued by the adiabatic shear decreases.

**Author contribution** Zhaocheng Wei's contributions to the research include leading the overall situation and conception. Wenyuan Wang's contributions to the research include conducting experiments, analyzing data, and writing articles. Biling Wang, Boyu Liu, and Hang Gao contributed to the experiment and data analysis. And Hang Gao contributed to the conception of the thesis. All authors participated in the reading and revision of the article and approved the final draft.

**Funding** This work is supported by National Key R & D Program Funded Project (2019YFA0705304), Key Fund Projects of National Natural Science Foundation of China (U1908231), and Fundamental Research Funds for the Central Universities (DUT21LAB107).

## Declarations

**Competing interests** The authors declare no competing interests.

## References

1. Kale A, Khanna N (2017) A review on cryogenic machining of super alloys used in aerospace industry[J]. Procedia Manuf 7:191–197
2. Deshpande YV, Andhare AB, Padole PM (2018) How cryogenic techniques help in machining of nickel alloys? A review[J]. Mach Sci Technol 22(4):543–584
3. Wang XJ, Meng L, Wen BC (2008) Development tendency and localization of large-scale centrifugal compressor of China[J]
4. Zhao L, Hu CG, Wu DX et al (2013) Research on milling parameters optimization and vibration test of FV520B steel [J]. Machine Tool Hydraulics 41(01):54–57
5. Chen JM, Huo HY, Hu CG (2014) Experimental study on high speed milling force of FV520B steel [J]. Fan Technol 56(5):58–61
6. Akgün M, Özlü B, Kara F (2022) Effect of PVD-TiN and CVD-Al2O3 coatings on cutting force, surface roughness, cutting power, and temperature in hard turning of AISI H13 Steel[J]. J Mater Eng Perform 1–12
7. AltanÖzbek N, Özbek O, Kara F et al (2022) Effect of eco-friendly minimum quantity lubrication in hard machining of Vanadis 10: a high strength steel[J]. Steel Res Int 93(7):2100587
8. Pimenov DY, Mia M, Gupta MK et al (2021) Improvement of machinability of Ti and its alloys using cooling-lubrication techniques: a review and future prospect[J]. J Mater Res Technol 11:719–753
9. Lubis SM, Darmawan'Adianto S (2019) Effect of cutting speed on temperature cutting tools and surface roughness of AISI 4340 steel[C]//IOP Conference Series: Materials Science and Engineering. IOP Publishing 508(1):012053
10. Hegab H, Umer U, Soliman M et al (2018) Effects of nano-cutting fluids on tool performance and chip morphology during machining Inconel 718[J]. Int J Adv Manuf Technol 96(9):3449–3458
11. Shi QH, Pan YZ, Fu XL et al (2021) Effect of anisotropy and cutting speed on chip morphology of Ti-6Al-4V under high-speed cutting[J]. Int J Adv Manuf Technol 113(9):2883–2894
12. Cui XB, Guo JX, Zhao J et al (2015) Chip temperature and its effects on chip morphology, cutting forces, and surface roughness in high-speed face milling of hardened steel[J]. Int J Adv Manuf Technol 77(9):2209–2219
13. Daymi A, Boujelbene M, Salem SB et al (2009) Effect of the cutting speed on the chip morphology and the cutting forces[J]. Arch Comput Mater Sci Surf Eng 1(2):77–83
14. Sun S, Brandt M, Dargusch MS (2010) Machining Ti-6Al-4V alloy with cryogenic compressed air cooling[J]. Int J Mach Tools Manuf 50(11):933–942
15. Liu NM, Chiang KT, Hung CM (2013) Modeling and analyzing the effects of air-cooled turning on the machinability of Ti–6Al–4V titanium alloy using the cold air gun coolant system[J]. Int J Adv Manuf Technol 67(5):1053–1066
16. Ren JL, Su Y, Guan XY et al (2010) Experimental study on the effect of cold air cutting on cutting temperature, cutting force and tool wear during machinging of Cr12 tool steel[C]//Key Engineering Materials. Trans Tech Publications Ltd 431:334–337

17. Brandt M, Sun S, Dargusch MS (2010) Machining Ti-6Al-4V alloy with cryogenic compressed air cooling[J]. Int J Mach Tools Manuf 50:933–942
18. Dhananchezian M, Kumar MP (2011) Cryogenic turning of the Ti–6Al–4V alloy with modified cutting tool inserts[J]. Cryogenics 51(1):34–40
19. Courbon C, Pusavec F, Dumont F et al (2013) Tribological behaviour of Ti6Al4V and Inconel718 under dry and cryogenic conditions—application to the context of machining with carbide tools[J]. Tribol Int 66:72–82
20. Karthik R, Malghan RL, Kara F et al (2021) Influence of support vector regression (SVR) on cryogenic face milling[J]. Adv Mater Sci Eng
21. Bermingham MJ, Kirsch J, Sun S et al (2011) New observations on tool life, cutting forces and chip morphology in cryogenic machining Ti-6Al-4V[J]. Int J Mach Tools Manuf 51(6):500–511
22. Bermingham MJ, Palanisamy S, Kent D et al (2012) A comparison of cryogenic and high pressure emulsion cooling technologies on tool life and chip morphology in Ti–6Al–4V cutting[J]. J Mater Process Technol 212(4):752–765
23. Chen C (2015) Design and experimental study of low temperature cutting device [D]. Nanjing University of Aeronautics and Astronautics, Nanjing
24. Ma JB (2010) Research on low temperature cutting of 1Cr18Ni9Ti austenitic stainless steel [D]. Taiyuan University of Science and Technology, Taiyuan
25. De Chiffre L, Andreasen JL, Lagerberg S et al (2007) Performance testing of cryogenic CO2 as cutting fluid in parting/grooving and threading austenitic stainless steel[J]. CIRP Ann 56(1):101–104
26. Machai C, Biermann D (2011) Machining of β-titanium-alloy Ti–10V–2Fe–3Al under cryogenic conditions: cooling with carbon dioxide snow[J]. J Mater Process Technol 211(6):1175–1183
27. Machai C, Iqbal A, Biermann D et al (2013) On the effects of cutting speed and cooling methodologies in grooving operation of various tempers of β-titanium alloy[J]. J Mater Process Technol 213(7):1027–1037
28. Sadik MI, Isakson S, Malakizadi A et al (2016) Influence of coolant flow rate on tool life and wear development in cryogenic and wet milling of Ti-6Al-4V[J]. Procedia CIRP 46:91–94
29. Jerold BD, Kumar MP (2013) The Influence of cryogenic coolants in machining of Ti–6Al–4V[J]. J Manuf Sci Eng 135(3):922–926
30. Qi XD (2017) Experimental study on cold milling of TC4 titanium alloy with dry ice [D]. Nanjing University of Aeronautics and Astronautics, Nanjing
31. Şirin Ş, Sarıkaya M, Yıldırım ÇV et al (2021) Machinability performance of nickel alloy X-750 with SiAlON ceramic cutting tool under dry, MQL and hBN mixed nanofluid-MQL[J]. Tribol Int 153:106673
32. Chen JJ, Wang Y, Zhang YF et al (2020) Investigation on tool wear mechanism during dry cutting 304 stainless steel[J]. Manuf Technol 20(1):36–44
33. Gao HH, Ma BJ, Zhu YP et al (2022) Enhancement of machinability and surface quality of Ti-6Al-4V by longitudinal ultrasonic vibration-assisted milling under dry conditions[J]. Measurement 187:110324
34. Dalimunthe FN, Ginting A (2020) MQL applied for hard machining of ferrous alloys using hardmetals: a review[C]//IOP Conference Series: Materials Science and Engineering. IOP Publishing 1003(1):012058
35. Pervaiz S, Anwar S, Qureshi I et al (2019) Recent advances in the machining of titanium alloys using minimum quantity lubrication (MQL) based techniques[J]. Int J Precis Eng Manuf-Green Technol 6(1):133–145
36. Sultana N, Dhar NR (2022) A critical review on the progress of MQL in machining hardened steels[J]. Adv Mater Process Technol 1–25
37. Wang XM, Li CH, Zhang YB et al (2022) Tribology of enhanced turning using biolubricants: a comparative assessment[J]. Tribol Int 107766
38. Liu MZ, Li CH, Zhang YB et al (2021) Cryogenic minimum quantity lubrication machining: from mechanism to application[J]. Front Mech Eng 16(4):649–697
39. Cui X, Li CH, Zhang YB et al (2022) Grindability of titanium alloy using cryogenic nanolubricant minimum quantity lubrication[J]. J Manuf Process 80:273–286
40. Yıldırım ÇV, Kıvak T, Sarıkaya M et al (2020) Evaluation of tool wear, surface roughness/topography and chip morphology when machining of Ni-based alloy 625 under MQL, cryogenic cooling and CryoMQL[J]. J Market Res 9(2):2079–2092
41. Qiao F, Ren F, Liu X et al (2018) Research on chip morphology in ultra-low temperature cutting of difficult-to-machine materials [J]. Mach Manuf (6)
42. Anqi AE, Li CH, Dhahad HA et al (2022) Effect of combined air cooling and nano enhanced phase change materials on thermal management of lithium-ion batteries[J]. J Energy Storage 52:104906
43. Li HK, Zhao PS (2013) Milling stability lobe diagram construction on FV520B stainless steel and experimental testing investigation[C]. Appl Mech Mater Trans Tech Publ Ltd 437:586–589
44. Yu HY (2012) Study on micro mechanism of chip formation in high speed cutting of stainless steel [D]. Dalian University of Technology, Dalian
45. Li GH (2009) Research on adiabatic shear prediction in high speed cutting based on linear disturbance analysis [D]. Dalian University of Technology, Dalian
46. Duan CZ, Liu YM, Sun W (2019) Influence of cutting parameters on cutting deformation of SiC_p/Al composites [J]. Tool Eng 53(01):20–24
47. Ni HC (2014) Calculation of shear angle in cutting process based on minimum energy principle [D]. Anhui Univ Technol
48. Zhou QQ, Yong XP, Li XY et al (2008) Study on low temperature properties of precipitate hardened FV520B steel [J]
49. Bao HS, Wang LL, Lu WX (1989) Explosion and shock waves, 9(2):109-119
50. Wang SP (2012) Microstructure and microhardness of adiabatic shear band of zigzag chip of TC4 titanium alloy [J]. China Mech Eng 023(009):1117–1121
51. Duan CZ, Wang MJ, Li GH et al (2007) Microstructure characteristics of adiabatic shear band in sawtooth chips in high speed cutting [J]. Explosion Shock Waves 01:91–99
52. Pan J, Qin M, Chen S (2017) Numerical investigation on the prefabricated crack propagation of FV520B stainless steel[J]. Results Phys 7:3738–3743